Structure, Vol. 9, 1225–1236, December, 2001, ©2001 Elsevier Science Ltd. All rights reserved. PII S0969-2126(01)00685-2

Crystallographic and Modeling Studies of RNase III Suggest a Mechanism for Double-Stranded RNA Cleavage

Jaroslaw Blaszczyk,[1] Joseph E. Tropea,[1] Mikhail Bubunenko,[2] Karen M. Routzahn,[1] David S. Waugh,[1] Donald L. Court, [2,3] and Xinhua Ji[1,3]

[1] Macromolecular Crystallography Laboratory
[2] Gene Regulation and Chromosome Biology Laboratory
Center for Cancer Research
National Cancer Institute
National Institutes of Health
Frederick, Maryland 21702

Summary

Background: *Aquifex aeolicus* Ribonuclease III (Aa-RNase III) belongs to the family of Mg^{2+}-dependent endonucleases that show specificity for double-stranded RNA (dsRNA). RNase III is conserved in all known bacteria and eukaryotes and has 1–2 copies of a 9-residue consensus sequence, known as the RNase III signature motif. The bacterial RNase III proteins are the simplest, consisting of two domains: an N-terminal endonuclease domain, followed by a double-stranded RNA binding domain (dsRBD). The three-dimensional structure of the dsRBD in *Escherichia coli* RNase III has been elucidated; no structural information is available for the endonuclease domain of any RNase III.

Results: We present the crystal structures of the Aa-RNase III endonuclease domain in its ligand-free form and in complex with Mn^{2+}. The structures reveal a novel protein fold and suggest a mechanism for dsRNA cleavage. On the basis of structural, genetic, and biological data, we have constructed a hypothetical model of Aa-RNase III in complex with dsRNA and Mg^{2+} ion, which provides the first glimpse of RNase III in action.

Conclusions: The functional Aa-RNase III dimer is formed via mainly hydrophobic interactions, including a "ball-and-socket" junction that ensures accurate alignment of the two monomers. The fold of the polypeptide chain and its dimerization create a valley with two compound active centers at each end of the valley. The valley can accommodate a dsRNA substrate. Mn^{2+} binding has significant impact on crystal packing, intermolecular interactions, thermal stability, and the formation of two RNA-cutting sites within each compound active center.

Introduction

Ribonuclease III (RNase III) belongs to the family of endoribonucleases that show specificity for double-stranded RNA (dsRNA) [1, 2] and is found in all studied prokaryotes and eukaryotes [2–6]. Three classes of RNase III enzymes have been reported, ranging in length from ~200 to ~2000 amino acid residues (Figure 1a). Class 1 enzymes are the simplest, containing an endonuclease domain and a dsRNA binding domain (dsRBD). Class 2 proteins contain two endonuclease domains and one dsRBD. Class 3 molecules consist of two endonuclease domains, one dsRBD, and an N-terminal helicase domain followed by a PAZ domain [6, 7]. The sequence of the endonuclease domain is characterized by the highly conserved 9 amino acid RNase III signature motif (Figure 1b). Class 1 RNase III from *E. coli* (Ec-RNase III) has been extensively studied [1, 8, 9]. Ec-RNase III influences the level of ~10% of all cellular proteins and affects the expression of many unrelated bacterial genes [10]. It influences gene expression by site-specific binding and cleavage of the messenger RNA (mRNA) (see review by Court, [2]). Ec-RNase III also participates in the maturation of ribosomal RNA (30S) precursors [11, 12]. Point mutations causing defects in this enzyme have been identified, and their effects were elucidated (Figure 1b). The active form of Ec-RNase III is a dimer of two identical 25-kDa polypeptides [1, 13], which degrades both natural and synthetic dsRNA to small duplex products ~10–18 nucleotides (nt) in length [2, 14–17], making RNase III a potential cellular defense against viral infection [1, 2, 18]. Recently, class 2 [6] and class 3 [7] RNase III proteins have been characterized. Structurally, class 3 enzymes have a helicase domain and a PAZ domain that are absent in class 2 proteins (Figure 1a). Functionally, class 3 enzymes produce discrete single-stranded RNA (ssRNA) products of ~22 nt from long dsRNA substrates, whereas class 2 proteins do not [7, 19]. The ~22-nt ssRNA segments act as guide RNAs, which mediate both RNA interference (RNAi) that destroys specific mRNAs [20] and the biogenesis of small temporal RNAs (stRNAs) that regulate stage-specific development [21, 22]. With accumulating genetic and biological findings, a three-dimensional structure of any RNase III enzyme should shed light on the mechanism of RNase III in RNA processing in general [2, 5, 23] and in RNAi and stRNA biogenesis in particular [7, 24].

The NMR solution structures of dsRBD in Ec-RNase III [25] and other types of dsRNA binding proteins have been reported [26–28]. In addition, a 1.9-Å crystal structure has been determined for a dsRBD of *Xenopus laevis* RNA binding protein A in complex with dsRNA [29]. These structures consistently show that three regions (region 1, 2, and 3) in the dsRBD (Figure 1b) are important for dsRNA recognition [28, 29]; point mutations of Ec-RNase III affecting regions 1 and 3 have been identified (Figure 1b).

Amino acid sequences have been reported for more than 40 RNase III proteins, among which 6 residues are strictly conserved (data not shown). According to the numbering scheme of the *Aquifex aeolicus* RNase III (Aa-RNase III), they are E40, G43, D44, E110, Y170, and

[3] Correspondence: court@ncifcrf.gov (D.L.C.), jix@ncifcrf.gov (X.J.)

Key words: RNase III; endonuclease domain; compound active center; dsRNA; RNA processing; RNA interference

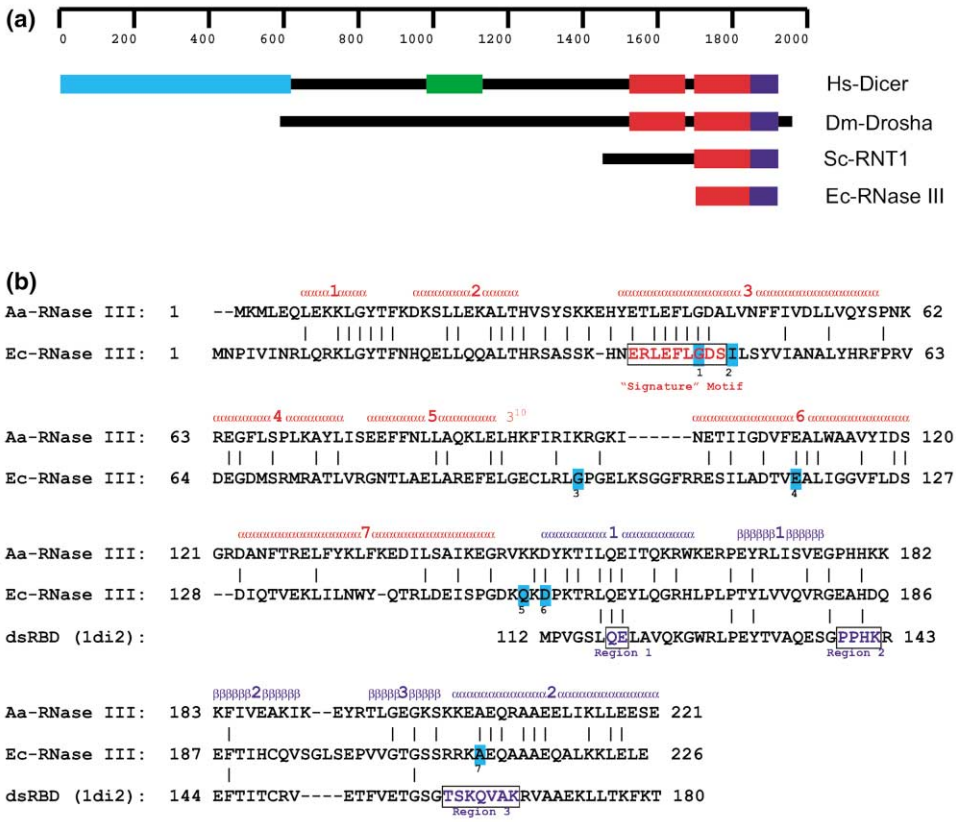

Figure 1. RNase III Proteins and Sequences

(a) Representatives of three classes of RNase III proteins: class 1 Ec-RNase III (SWISS-PROT P05797) and *Saccharomyces cerevisiae* RNT1 (Sc-RNT1, SWISS-PROT Q02555), class 2 *Drosophila melanogaster* Drosha (Dm-Drosha, SWISS-PROT Q9XYN5), and class 3 *Homo sapiens* Dicer (Hs-Dicer, GenBank AB028449). The scale on top indicates the lengths of polypeptide chains. The cyan box represents the helicase domain, the green box represents the PAZ domain, the red box represents the endonuclease domain, and the blue box represents the dsRBD.

(b) Sequence alignment of Aa-RNase III, Ec-RNase III, and the dsRBD of *X. laevis* RNA binding protein A [29]. The secondary structure assignment shown on top of the sequences is based on the crystal structure of the endonuclease domain of Aa-RNase III (in red, this work) and the crystal structure of the dsRBD of *X. laevis* protein in complex with dsRNA (in blue) [29]. The boxed regions include the RNase III signature motif [2, 6] and three areas that are involved in dsRNA recognition [29]. Cyan-shaded amino acid residues are seven known point mutations of Ec-RNase III: 1, G → D (rnc105, [58, 59]); 2, I → N (*rnc*⁻, H.K. Peters, N. Costantino, and D.L.C., unpublished data); 3, G → E (rnc97, [38]); 4, E → K (rnc70, [34, 35, 37]), E → A [35], and E → Q and E → D [36]; 5, Q → P (rnc10, [60]); 6, D → E (rnc7, [60]); and 7, A → V (rev3, [58]).

(c) Sequence alignment of proposed RNA-cutting site residues. One representative is shown for each of the three RNase III classes, including class 1 Aa-RNase III (SWISS-PROT O67082), class 2 Dm-Drosha (SWISS-PROT Q9XYN5), and class 3 Hs-Dicer (GenBank AB028449). The proposed RNA-cutting residues are shown in red. The vertical lines indicate residues conserved in all five endonuclease domains. The numbering on top is that of Aa-RNase III; numbering for each protein is provided on the side of each sequence stretch. The existence or absence of dsRBD is indicated by a "+" or "−" sign, respectively.

A210; residues E40, G43, and D44 are located in the signature motif. In addition, 27 other residues are identical in more than 30 sequences (data not shown), among which R38, L39, F41, and L42 are also found in the signature motif (Figures 1b and 1c). In contrast to the relatively rich structural information for the dsRBD, no

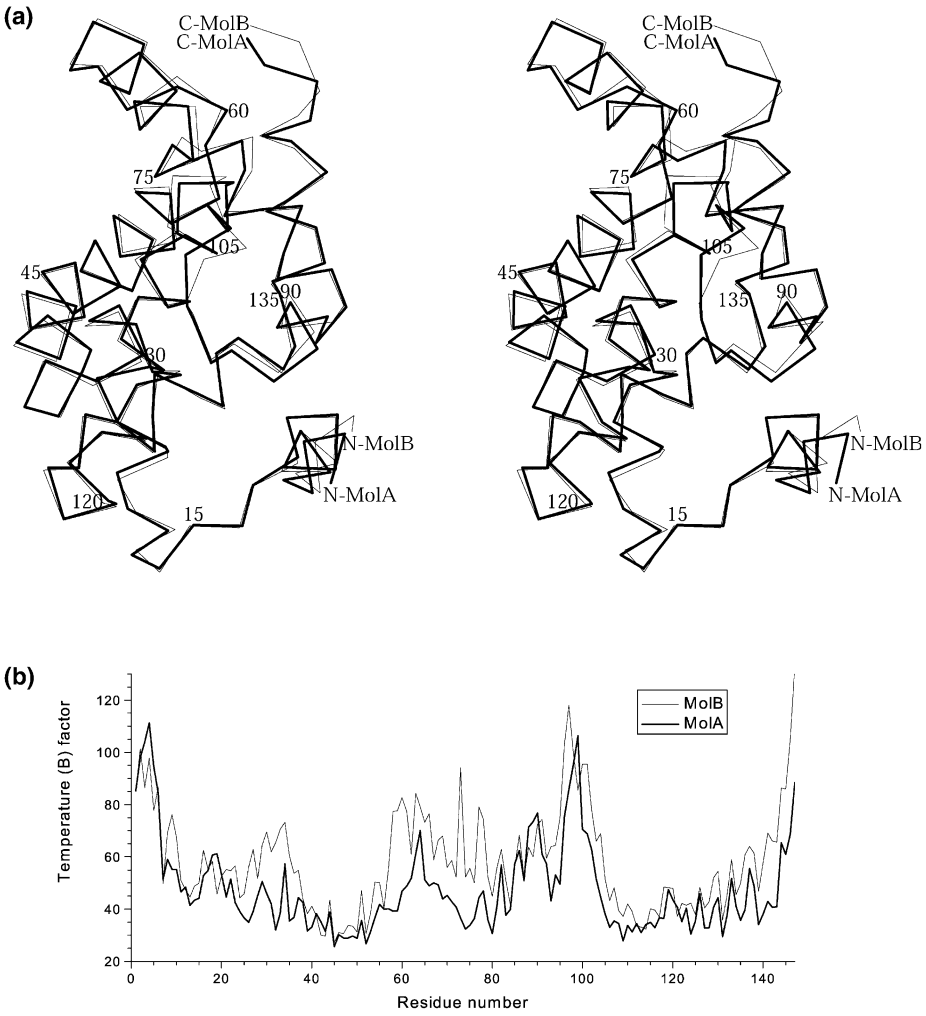

Figure 2. Comparison of the Two Endonuclease Domains in the Dimeric Ligand-free Aa-RNase III

(a) Cα-trace superposition of molecules A (thick lines) and B (thin lines).

(b) Relative mobility as indicated by the residue-averaged temperature (B) factors. The average B factor for molecule A (thick lines) is 47.7 Å^2, and that for molecule B (thin lines) is 59.0 Å^2. The average B factor for the structure including solvent molecules is 54.4 Å^2, consistent with the estimated value using Wilson plot (48.0 Å^2).

structure has been reported for the endonuclease domain. It has been demonstrated, however, that the stand-alone endonuclease domain of Ec-RNase III cleaves dsRNA in vitro [4], suggesting that the stand-alone endonuclease domain must be able to weakly bind dsRNA without dsRBD. We present here the crystal structure of the N-terminal endonuclease domain of Aa-RNase III, containing residues 1–147 (Figures 1b and 2a). To probe the active center of Aa-RNase III, we also determined the crystal structure of its endonuclease domain in complex with Mn^{2+} or Mg^{2+} ion.

Our structures provide the first view of an RNase III endonuclease domain, reveal a novel protein fold, and suggest a mechanism for dsRNA cleavage. RNase III is known to function as a dimer. We show that the dimer is formed in the endonuclease domain by hydrophobic interactions. A ball-and-socket junction secures the relative positions of the two subunits (Figure 3a). A valley is created at the subunit interface (Figure 3c) of the size to accommodate a dsRNA substrate. The fold of the individual polypeptide chains and the joining of two subunits by dimerization bring together six negatively charged side chains to form a compound active site at each end of the RNA valley (Figure 3b). Metal binding results in the resolution of two RNA-cutting sites within each compound active center (Figure 4a). Our genetic analysis studies demonstrate that all of the four residues identified as being at the RNA-cutting site are critical to cellular RNase III function in the *E. coli* protein. Our structure-based modeling studies (Figures 5 and 6) provide the first view of an RNase III enzyme in action, shedding light on the catalytic mechanism of not only class 1 RNase III enzymes but also class 2 and 3 proteins.

Results

A Novel Helical Protein Fold

The crystal structure shows that the novel fold of the Aa-RNase III endonuclease domain is 70% helical, containing seven α helices and a 3_{10} helix, but no β strands

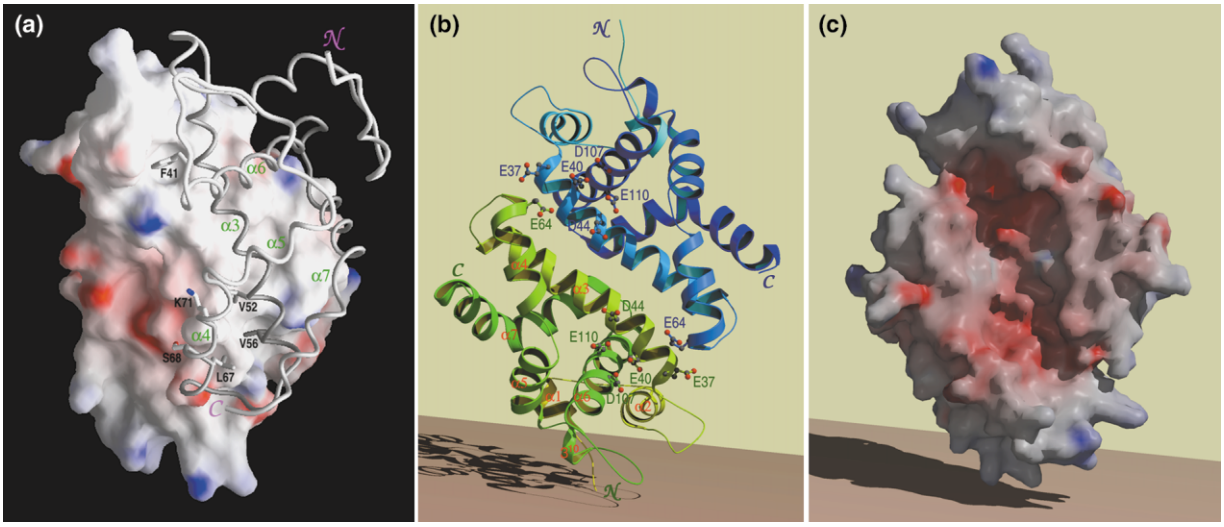

Figure 3. Structure of the Ligand-free Dimer of Aa-RNase III Endonuclease Domain

(a) Dimer interface of Aa-RNase III. Molecule A is illustrated as a surface representation with positive and negative potentials indicated by blue and red, respectively. Molecule B is represented as a backbone "worm" with a stick model for the "ball-and-socket" side chains. The secondary structure elements involved in dimerization are identified with green labels. In the upper portion of the illustration, the shape of the "socket" is shown with the stick model of F41 from Molecule B, whereas, in the lower potion, the shape of the "ball" is outlined in the middle of five side chains that form the socket (see text).

(b) A ribbon diagram of molecules A (in green) and B (in blue). The secondary structure assignment is shown in molecule A only. Two sets of six active site residues are labeled, including E37, E40, D44, D107, and E110 from one molecule and E64 from the other. Each set forms a compound active center.

(c) A surface representation with red and blue indicating negative and positive potentials, respectively. Notice that the valley on the surface of the dimer has one compound active center on each end of the valley. The representations were prepared using MOLSCRIPT [61], GRASP [62], and Raster3D [63].

(Figures 1b and 2a). No similar fold was found in a topological search using DALI (EMBL, Heidelberg, Germany).

There are two crystallographically independent molecules, A and B, in the asymmetric unit of the ligand-free structure (Figure 2a). The rmsd for all 147 pairs of Cα positions is 0.71 Å, whereas it is 0.48 Å when the alignment is optimized for 142 pairs of Cα atoms. The excluded Cα atoms for optimized alignment are residues 1–2 (N terminus), 98, and 146–147 (C terminus, see Figure 2a). These three regions are highly flexible, as indicated by their high local mobility (Figure 2b) and poor electron density (not shown).

A Dimer with Two "Ball-and-Socket" Junctions and a Large Valley

The structure shows that molecules A and B form a tight dimer. The dimer interface is a hydrophobic surface (Figure 3a). A total of 128 hydrophobic interactions (<4.0 Å) are found between A and B, whereas only 20 hydrogen bonds/salt bridges exist at the dimer interface. The secondary structural elements involved in dimerization include nearly all of α3 (residues 37–38, 41–42, 45–46, 48–49, 52–53, and 56–57) and α4 (residues 62–64, 67–68, and 71), the C terminus of α6 (residue 117), and the N terminus of α7 (residues 122–125 and 128) (Figure 3a and 3b). Identical "ball-and-socket" junctions are formed at each end of the dimer interface (Figure 3a). The "ball" is the side chain of F41 from molecule A (B), and the "socket" is a cavity formed by side chains V52, V56, L67, S68, and K71 from molecule B (A). This type of "locking" device is well documented for another dimeric enzyme, glutathione S-transferase [30–32]. The two α3 helices from molecules A and B are antiparallel along the entire dimer interface (Figure 3b), forming the bottom of a valley, 50 Å long and 20 Å wide, which can accommodate a dsRNA substrate (Figure 3c).

To assess the importance of this ball-and-socket interaction, five site-directed mutants of Ec-RNase III were constructed and tested in the λ*N-lacZ* assay [33, 34] for RNase III activity: F40G, F40D, F40R, F40M, and F40W (F40 in *E. coli* corresponds to F41 in Aa-RNase III). The F40G, F40D, and F40R substitutions gave rise to a defective enzyme, whereas the F40M and F40W mutants were functional in the assay. We conclude that the hydrophobic side chains of the latter mutants can still function as the ball in the ball-and-socket junction, but this interaction is precluded by the charged side chains (F40D and F40R) or in the absence of any side chain in this position (F40G).

A Compound Active Center at Each End of the Valley

The fold within each molecule groups D107 and E110 with three other negatively charged residues, E37, E40, and D44, which are part of the signature motif (Figure 3b). In the ball-and-socket junctions, the ball (F41) is located in the middle of the RNase III signature motif (Figure 1b). Therefore, the two junctions secure the relative positions of the two signature motifs in the dimer. In addition, the ball-and-socket junction juxtaposes residue E64 from molecule B (A) with the signature motif of molecule A (B). Thus, including E64, six negatively

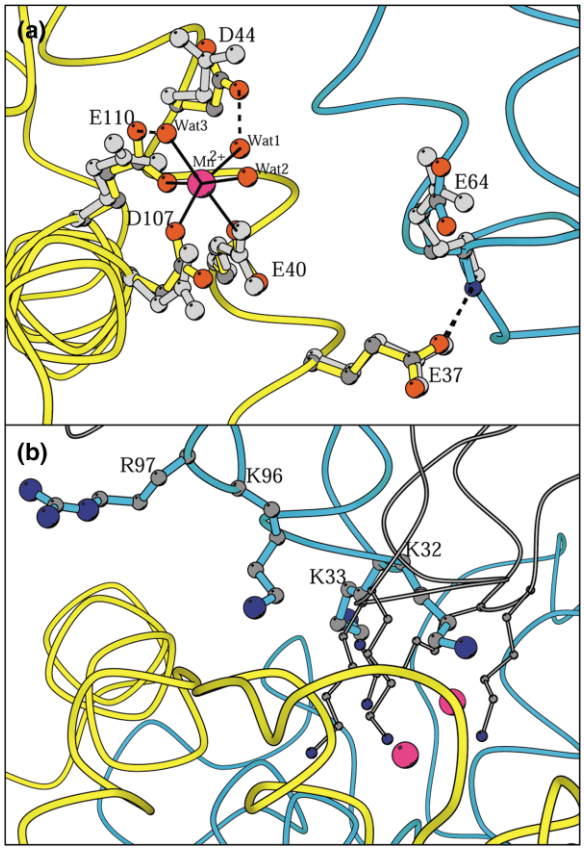

Figure 4. Mn^{2+} Coordination and the Impact of Mn^{2+} Binding

(a) Compound active center and the Mn^{2+} coordination in Aa-RNase III. Molecule A is shown in yellow, and molecule B is shown in blue. Side chains in the Mn^{2+}-bound structure are illustrated by atomic color (carbon in dark gray, nitrogen in blue, and oxygen in red); side chains in the ligand-free structure are in gray. The Mn^{2+} coordination is illustrated using solid lines, and hydrogen bonds are illustrated with dashed lines.

(b) Crystal packing and the impact of Mn^{2+} binding. The yellow (molecule A) and blue (molecule B) diagrams represent the Mn^{2+}-bound dimeric endonuclease domain of Aa-RNase III. The side chains of K32, K33, K96, and K97 are from molecule B (in blue) of another dimeric molecule. In the ligand-free protein, the four positively charged side chains from a symmetry-related dimer (in gray) penetrate deeply into the valley. For clarity, only the symmetry-related dimer of the ligand-free protein is shown. The illustration was prepared using MOLSCRIPT [61].

charged side chains are clustered at each end of the dimer interface. These clusters are likely to represent two compound active centers of the protein (Figure 3b); it is known that E117 in *E. coli* (E110 in *A. aeolicus*) is important for phosphodiester hydrolysis [35] and metal binding [36].

Mn^{2+} Binding Site and Mn^{2+}-Induced Changes

The concentration of the negative charges in the valley (Figure 3c) leads to a highly dynamic dimer in the ligand-free state, which can be stabilized by the binding of metal ions. Mn^{2+} mimics Mg^{2+} when it binds to protein; Mn^{2+} is heavier than Mg^{2+} and is easier to identify in X-ray diffraction analysis. Therefore, Mn^{2+} is often used to probe the Mg^{2+} binding sites in protein crystallography. Initial soaking of ligand-free crystals in Mn^{2+}-containing buffer resulted in the loss of X-ray diffraction. Subsequently, crystals for structure determination have been obtained by crystallizing the enzyme in the presence of Mn^{2+} ions. We have also obtained crystals of the endonuclease domain of Aa-RNase III in complex with Mg^{2+}. The crystal structure of the Mg^{2+}-bound protein (J.B. and X.J., unpublished data) proves that the Mg^{2+} binding site is the Mn^{2+} binding site with identical coordination (data not shown). In the following structural analysis, we use the Mn^{2+} complex because it has higher resolution (2.1 Å) than the Mg^{2+} complex (2.3 Å).

The binding of Mn^{2+} causes significant conformational changes of the side chains of D44, D107, and E110 (Figure 4a). However, it does not affect the side chain conformation of E40, probably because E40 is adjacent to F41 and is restrained by the ball-and-socket junction (Figure 3a and 3b). E37 does not change its side chain conformation either, possibly because its carboxylate group forms a strong hydrogen bond with the amide group of E64 across the dimer interface (Figure 4a). The Mn^{2+} ion has six coordinates, three with the side chains of E40, D107, and E110, and three with water molecules (Figure 4a). Residue E110 interacts with Mn^{2+}, as predicted by Sun and Nicholson [36], and also interacts with one of the three water molecules, whereas residue D44 interacts only with a water molecule. Residues E40 and D44 are part of the RNase III signature motif; D107 and E110 are located in helix α6 (Figure 1b). In *E. coli*, the point mutation *rnc70* changes the E117 codon to a lysine codon (E110 in *A. aeolicus*, see Figure 1b). This mutant of Ec-RNase III fails to cleave dsRNA but still binds the dsRNA substrate [34, 37].

The presence of Mn^{2+} changes the dimer-dimer interaction in the crystals of Aa-RNase III. In the crystal lattice of ligand-free dimers, the clustered negative charges in the valley of one dimer are neutralized by four positively charged side chains from an adjacent dimer (Figure 4b). In contrast, when Mn^{2+} is bound, these four side chains are either withdrawn or point away from the Mn^{2+} binding site (Figure 4b). Mn^{2+} binding causes the dimer to be more thermally stable. The drop of the crystallographic temperature factors (B factors) is $\sim$20 Å^2 and is consistent over the entire polypeptide chain, except for the region near residue 98 where the B factor drop reaches $\sim$60 Å^2. It is known that RNase III is a Mg^{2+}-dependent enzyme [2–4, 16]. In the region near residue 98, a point mutant G → E (*rnc97*) was discovered in *E. coli*, for which the limitation of Mg^{2+} ions in vivo appeared to be responsible [38]. Our findings support this hypothesis in that Mn^{2+} binding causes significant stabilization of the local mobility in this region, reinforcing the notion that the position of Mn^{2+} is where Mg^{2+} binds.

Two RNA-Cutting Sites within Each Compound Active Center

The net effect of ion coordination is to tightly organize the six negatively charged residues at each end of the valley into two groups, E40/D44/D107/E110 and E37/E64 (Figures 3b and 4a), creating the potential for two RNA-cutting sites within each compound active center. Note that E110 is located in one of the two RNA-cutting

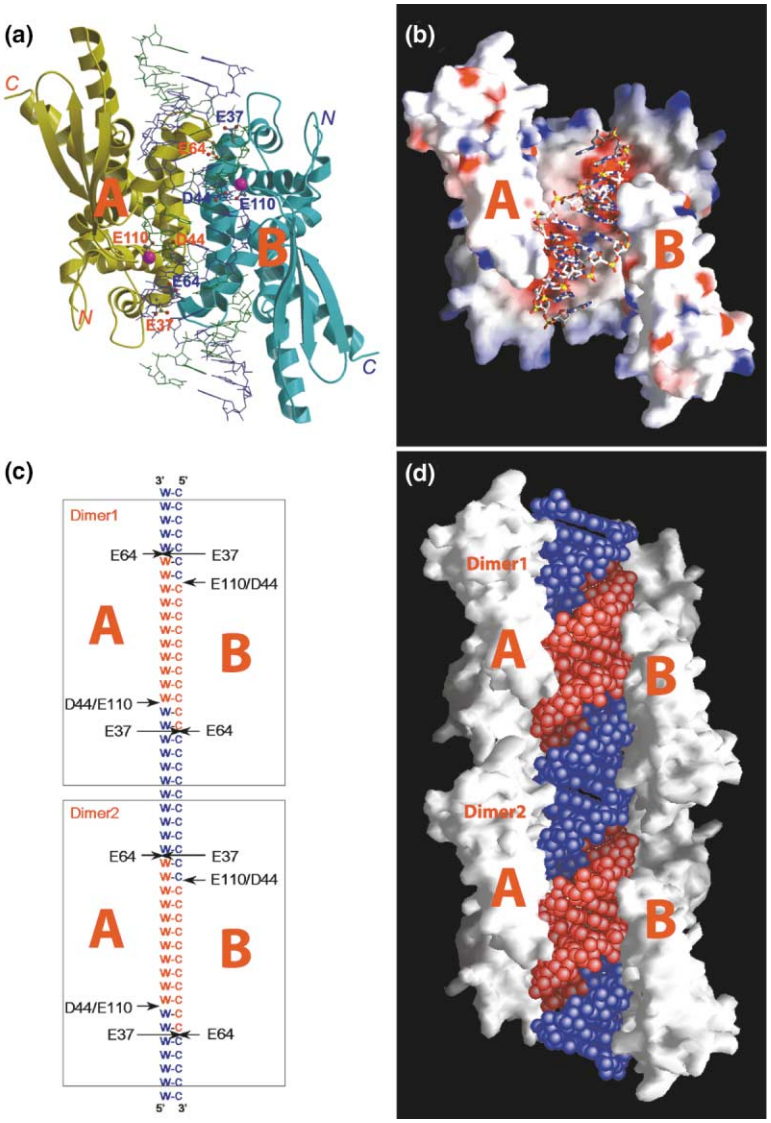

Figure 5. The Proposed Mechanism of dsRNA Cleavage by Class 1 RNase III

(a) A hypothetical model of the Aa-RNase III/Mg^{2+}/dsRNA complex. Protein is illustrated as ribbons, dsRNA is illustrated as sticks, and Mg^{2+} is illustrated as purple spheres. Molecule A is in yellow, and molecule B is in cyan. The RNA strand associated with molecule A is in green, and the strand associated with molecule B is in blue. Residues E37, D44, E64, and E110 are labeled in red for molecule A and in blue for molecule B.

(b) A model of Aa-RNase III in complex with the product of dsRNA cleavage. The protein is shown as a surface representation with positive potential indicated in blue and negative potential indicated in red. The product is shown as a stick model with an atomic coloring scheme (carbon in white, nitrogen in blue, and oxygen in red).

(c) A model of two dimeric Aa-RNase III molecules that bind and cut a dsRNA, producing identical RNA products (distinguished with alternate colors), each containing a 9-bp dsRNA segment with a 2-base 3′ overhang at each end of the segment.

(d) A space-filling model of (c). Protein is illustrated as a surface representation; dsRNA products are shown as van der Waals spheres with alternate colors. The illustration was prepared using MOLSCRIPT [61], GRASP [62], and Raster3D [63].

sites. This residue in *E. coli* is important for phosphodiester hydrolysis [35]. Note also that, on a long duplex RNA substrate, each dimeric RNase III would have the potential to make double-stranded cleavages at each of its two compound active centers, i.e., four cleavages per dimer.

A Hypothetical Model of Aa-RNase III/Mg^{2+}/dsRNA Suggests Four RNA-Cutting Residues

The shape and dimensions of the valley, the location of the two compound active centers, and the two Mg^{2+} binding sites indicate that the valley accommodates the dsRNA. Assuming this feature is correct, we have built a model of a full-length Aa-RNase III in complex with dsRNA, starting with the endonuclease domain structure and the structure of dsRBD in complex with dsRNA [29]. The complete model contains two full-length Aa-RNase III protein molecules, two Mg^{2+} ions, and a dsRNA substrate of 23 base pairs (bp) (Figure 5a).

Our model of Aa-RNase III/Mg^{2+}/dsRNA suggests that, at each compound active center, two hydrolysis events cleave the dsRNA two bases apart, generating a 3′ overhang (Figure 5a). The distal RNA-cutting site that generates the 3′ overhang is composed of residues E37 from one molecule and E64 from the other molecule of the dimer. The second cutting site 2 bp toward the center of the dimer is composed of residues D44 and E110 (Figure 5a and 5b). Residue E110 corresponds to E117 in *E. coli*, which is known to be essential for the catalytic cleavage of dsRNA by Ec-RNase III [34, 35, 37]. Our site-directed mutants E38V, D45A, and E65A of Ec-RNase III (E37, D44, and E64 in AaRNase III, see Figure 1b) demonstrate that these three residues are also essential for RNase III activity, as determined by an in vivo assay. Thus, all of the four residues proposed for RNA cleavage are critical to the function of cellular RNase III.

Discussion

Proposed Mechanism for Class 1 RNase III

It is known that RNase III cleaves phosphodiesters to provide 5′-phosphate, 3′-hydroxyl termini with a 2-base 3′ overhang (for reviews see [2, 3, 16]). Based on our

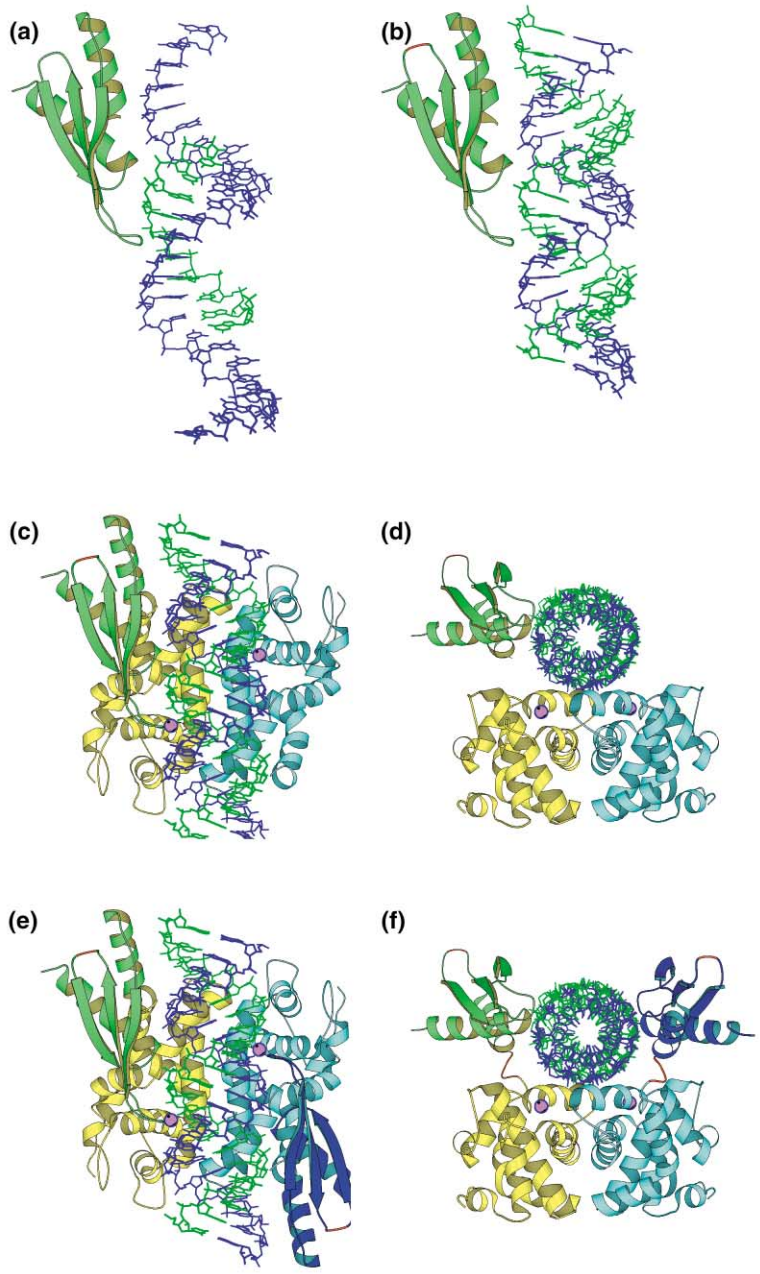

Figure 6. The Construction of the Aa-RNase III/Mg^{2+}/dsRNA Complex

(a) The 1.9-Å crystal structure of the *X. laevis* dsRBD/dsRNA complex [29].

(b) The model of an *A. aeolicus* dsRBD with a dsRNA substrate containing 23 bp. Two residues (191–192, see Figure 1b) were inserted (shown in red).

(c) The model of two *A. aeolicus* endonuclease domains (crystal structure), one *A. aeolicus* dsRBD, and a 23-bp dsRNA.

(d) Same as (c), with a 90° rotation around the horizontal axis.

(e) The model of dimeric Aa-RNase III in complex with the 23-bp dsRNA. Note that the dsRBD-dsRNA interactions as found in the crystal structure of *X. laevis* dsRBD/dsRNA [29] are maintained for both dsRBDs.

(f) Same as (e), with a 90° rotation around the horizontal axis. The three residues shown in red (148–150, see Figure 1b) were modeled between the endonuclease domain and dsRBD. Protein is illustrated as ribbons, dsRNA is illustrated as sticks, and Mg^{2+} is illustrated as purple spheres. Molecule A is in yellow (endonuclease domain) and green (dsRBD), and molecule B is in cyan (endonuclease domain) and blue (dsRBD). Red loop segments are the inserted residues. The RNA strand associated with molecule A is in green, and the strand associated with molecule B is in blue. The illustration was prepared using MOLSCRIPT [61] and Raster3D [63].

model, a long dsRNA duplex is cut at four places by one dimeric class 1 RNase III. The four cleavages create a 9-bp dsRNA segment with a 2-base overhang at each 3′ hydroxyl end. This RNA would have a total length of 13 nt (9+2+2), created by the two overlapping strands of 11 nt each (Figure 5b).

The complete digestion of dsRNA may be achieved by the collective binding and cleavage by many dimeric molecules. A model of two such dimers binding and cleaving the dsRNA is illustrated in Figure 5 ([c] and [d]). The valley of each dimer accommodates 21 bp of a dsRNA substrate. We suggest that two dimers share one more bp between them (Figure 5c). As such, the two dimers could produce 3 dsRNAs, each of 9 bp with a 2-base overhang at each end of the 9-bp dsRNA segment (Figure 5d). If many dimers bind and cleave, the dsRNA duplex could be processed to completion. Theoretically, the products could uniformly be the 9-bp dsRNA segments with a 2-base 3′ overhang at each end, containing two strands of 11 nt. In fact, however, class 1 RNase III proteins also generate longer products [39, 40], which may be created when the gap between the RNase III dimers varies due to sequence specificity or inhibitory Watson-Crick bp sequences [4]. Nevertheless, our model suggests that a 9-bp dsRNA segment with a 2-base 3′ overhang at each end and containing two strands of 11 nt (i.e., a total length of 13 nt) could be produced internally by every dimer (Figure 5c and 5d). In summary, the product of class 1 RNase III cleavage could be a mixture of dsRNA segments of (9+n)-bp with a 2-base 3′ overhang at each end, containing two strands of (11+n) nt, where n equals 0,1,2....

Table 1. Crystal and X-Ray Diffraction Data of Native, Heavy-Atom Derivatives, and the Mn^{2+} Complex of the Endonuclease Domain of Aa-RNase III

	Native	Au Derivative	U Derivative	Mn^{2+} Complex
Crystal dimensions (mm)	0.10 × 0.15 × 0.25	0.10 × 0.10 × 0.20	0.10 × 0.10 × 0.20	0.20 × 0.20 × 0.25
Resolution (Å)	2.15	3.00	2.90	2.10
Space group	$P2_12_12_1$	$P2_12_12_1$	$P2_12_12_1$	$P2_1$
Unit cell dimensions: a (Å)	46.16	46.40	46.49	49.74
b (Å)	51.12	51.89	51.60	140.55
c (Å)	123.47	124.72	118.40	49.76
β (°)	90	90	90	117.42
Measured reflections	68,832	23,588	28,927	72,740
Unique reflections	16,542	11,071	12,404	33,591
Overall completeness (%)	99.5	96.2	98.4	92.9
Last shell[a] completeness (%)	99.9	89.7	93.8	74.7
Overall R_{sym}[b]	0.038	0.054	0.054	0.059
Last shell R_{sym}	0.370	0.235	0.446	0.185
Overall $I/\sigma(I)$	23.4	18.2	11.3	10.3
Last shell $I/\sigma(I)$	3.3	3.5	1.7	3.0

[a] 2.23–2.15 Å for native, 3.11–3.00 Å for the Au derivative, 3.00–2.90 Å for the U derivative, and 2.18–2.10 for the Mn^{2+} complex.
[b] $R_{sym} = \Sigma|(I - <I>)|/\Sigma(I)$, where I is the observed intensity.

Functional Implications for Class 2 and 3 RNase III Proteins

Class 2 and 3 RNase III proteins have two endonuclease domains per molecule (Figure 1a). However, the two endonuclease domains are different. The first endonuclease domain of both class 2 and 3 proteins has all four RNA-cutting residues conserved, whereas the second endonuclease domain does not (Figure 1c). In the second endonuclease domain of class 2 protein, Q1012 is the residue corresponding to E37 in Aa-RNase III. In class 3 enzyme, Q1704 and P1731 correspond to Aa-RNase III's E37 and E64, respectively (Figure 1c). Note that E37 and E64 form one RNA-cutting site across the dimer interface (Figure 4a). This class-dependent feature may be important for the function of class 2 and 3 enzymes. It is known that both RNAi [24, 41–43] and stRNAs biogenesis [21, 22] are characterized by the generation of ssRNAs of ~22 nt. It is also known that

Table 2. Structure Solution and Refinement of Aa-RNase III Endonuclease Domain in Its Ligand-free Form and in Complex with Mn^{2+}

	Ligand-Free	Mn^{2+}-Bound
Structure Solution		
Method	MIR	MR
Number of heavy atom sites found	Au: 2; U: 1	n/a[a]
Mean figure of merit:		
After SOLVE run	0.429	n/a
After SHARP solvent flipping	0.751	n/a
After DM NCS averaging	0.915	n/a
Correlation coefficient	n/a	0.63
R factor	n/a	0.38
Structure Refinement		
Resolution (Å)	30.0–2.15	30.0–2.10
Dimeric molecules in the asymmetric unit	1	2
Solvent content (%)	36.3	39.7
Matthews coefficient ($Å^3$/Da)	2.01	2.13
Data used for refinement $I \geq 2\sigma(I)$/all	13,894/15,686	26,642/31,456
Data used for R_{free} calculations, $I \geq 2\sigma(I)$/all	718/783	1,461/1,725
Number of least-squares parameters	9,323	22,954
Number of residues/(non-H) atoms	294/2,444	604/5,052
Number of water oxygen atoms	252	712
Number of heterogen atoms	0	4 Mn^{2+} ions
Final R, $I \geq 2\sigma(I)$/all	0.207/0.222	0.191/0.209
Final R_{free}, $I \geq 2\sigma(I)$/all	0.263/0.275	0.256/0.277
Rmsd (Å): bond lengths	0.005	0.005
Angle distances	0.018	0.018
Estimated coordinate error (Å)	0.26	0.23
Ramachandran plot: most-favored regions	91.2	91.4
Allowed	8.1	6.8
Generous	0.7	1.8
Disallowed	0.0	0.0

[a] Not applicable.

class 2 RNase III does not produce these ssRNAs, whereas class 3 enzyme does [7]. This difference may be the consequence of the unique variation (P1731, see Figure 1c) occurring in the second endonuclease domain of class 3, but not class 2, RNase III proteins.

The crystal structure of the *A. aeolicus* endonuclease domain reveals that the polar acidic side chain of E37 forms a strong hydrogen bond with the amide group of E64 (Figure 4a), which is functionally essential, as suggested by the defective site-directed mutant E38V of Ec-RNase III (E37 in Aa-RNase III), which cannot form this hydrogen bond. In contrast, a glutamine variation at this position may not destroy the E37/E64-cutting site, because it can form a hydrogen bond with the amide group of E64 (E65 in Ec-RNase III). Our site-directed E → Q mutation at this position of Ec-RNase III indeed causes no genetic defect in RNase III function. Therefore, the class 2 and class 3 endonuclease domain with a glutamine at this position (Q1012 in class 2 and Q1315 in class 3, respectively, see Figure 1c) might not lead to a defective RNase III function.

Our genetic analysis demonstrated that the mutations E65A and E65P in Ec-RNase III (E64 in Aa-RNase III) disabled RNase III function. Therefore, the proline residue at this position of class 3 RNase III (P1737) may disable the compound active center formed across the dimer interface. In summary, our working hypothesis is that class 2 RNase III may not have defective cutting sites and therefore may produce dsRNA fragments with two strands of ~11 nt and that class 3 proteins may have alternate disabled active centers and produce dsRNA fragments with two strands of ~22 nt.

Biological Implications

RNase III is a double-stranded RNA (dsRNA)-specific endonuclease, conserved in all known bacteria and eukaryotes and having a characteristic signature motif. The bacterial RNase III proteins are the simplest, consisting of two domains: an N-terminal endonuclease domain, followed by a double-stranded RNA binding domain (dsRBD). The three-dimensional structure of the dsRBD in *Escherichia coli* RNase III has been elucidated by NMR; no structural information is available for the endonuclease domain of any RNase III. We present here the crystal structure of the N-terminal endonuclease domain of RNase III from *Aquifex aeolicus* (Aa-RNase III). To probe the active center of Aa-RNase III, we also determined the crystal structure of its endonuclease domain in complex with Mn^{2+} or Mg^{2+} ion. Our structures provide the first view of an RNase III endonuclease domain and reveal a novel protein fold. RNase III is known to function as a dimer. We show that the dimer is formed in the endonuclease domain by hydrophobic interactions. A ball-and-socket junction secures the relative positions of the two subunits. A valley is created at the subunit interface of the size to accommodate a dsRNA substrate. The fold of the individual polypeptide chains and the joining of two subunits by dimerization bring together six negatively charged side chains to form a compound active site at each end of the RNA valley. Metal binding results in the resolution of two RNA-cutting sites within each compound active center. Our genetic analysis studies demonstrate that all of the four residues identified as being at the RNA-cutting site are critical to cellular RNase III function in the *E. coli* protein. Our modeling studies based on our structures and the structure of a dsRBD/dsRNA complex provides the first view of an RNase III enzyme in action, suggesting a mechanism for dsRNA cleavage. On a long duplex RNA substrate, each dimeric RNase III would have the potential to make double-stranded cleavages at each of its two compound active centers, i.e., four cleavages per dimer, producing a 9-bp dsRNA segment with a 2-base 3′ overhang at each end and containing two strands of 11 nt (i.e., a total length of 13 nt).

Experimental Procedures

Protein Expression and Purification

The open reading frame (ORF) encoding the endonuclease domain (residues 1–147) of Aa-RNase III (GenBank accession: AAC07049) was amplified from genomic DNA by the polymerase chain reaction (PCR) using the following oligonucleotide primers: 5′-GAGAACCTG TACTTCCAGGGTATGAAAATGTTGGAGCAACTTG-3′ and 5′-ATTA GTGATGATGGTGGTGATGTCTTCCCTCTTTTATAGCACTCAG-3′. This PCR amplicon was subsequently used as the template for a second PCR with the following primers: 5′-GGGGACAAGTTTGTA CAA AAAAGCAGGCTCGGAGAACCTGTACTTCCAG-3′ and 5′-GGG GACCACTTTGTACAAGAAAGCTGGGTT ATTAGTGATGATGGTGG TGATG-3′. The amplicon from the second PCR was inserted by recombinational cloning into the entry vector pDONR201 (Invitrogen) to create pKM801, and the nucleotide sequence of the entire insert was confirmed experimentally. Next, the RNase III endonuclease domain ORF, now bracketed by a hexahistidine tag on its C terminus and a recognition site for tobacco etch virus (TEV) protease (ENLYFQG) on its N terminus, was moved from pKM801 by recombinational cloning into the destination vector pKM596 [44] to produce pKM803. pKM803 directs the expression of the Aa-RNase III endonuclease domain in the form of an "affinity sandwich", with *E. coli* maltose binding protein (MBP) and a polyhistidine tag fused to its N and C termini, respectively. The MBP moiety can be removed by cleaving the fusion protein with TEV protease at a designed site in the linker to yield a recombinant Aa-RNase III endonuclease domain protein with a hexahistidine tag on its C terminus and a single nonnative glycine residue added to its N terminus. The fusion protein was expressed in *E. coli* BL21-RIL cells (Stratagene). Cells containing the expression vector were grown to mid-log phase ($OD_{600} = 0.5$) in LB broth [45] containing 100 μg/ml ampicillin and 30 μg/ml chloramphenicol, at which time isopropyl-β-D-thiogalactopyranoside (IPTG) was added to a final concentration of 1 mM. 4 hr after induction, the cells were pelleted by centrifugation and stored at −80°C.

E. coli cell paste was suspended in ice-cold 50 mM sodium phosphate (pH 8) 300 mM NaCl buffer (buffer A) containing the complete protease inhibitor cocktail (Roche Molecular Biochemicals) and disrupted with an APV Gaulin Model G1000 homogenizer at 10,000 psi. The homogenate was centrifuged at 20,000 × g for 30 min at 277K, and the supernatant was heat treated at 348K for 20 min. After pelleting the insoluble material by centrifugation, the supernatant was filtered through a 0.45-μm cellulose acetate membrane and applied to a 10-ml Ni-NTA Superflow affinity column (Qiagen) equilibrated in buffer A. The column was washed with 10 column volumes of equilibration buffer and 10 column volumes of buffer A containing 25 mM imidazole to remove nonspecifically-bound protein. Elution was carried out with a linear gradient from 25 to 250 mM imidazole in buffer A. Fractions containing recombinant Aa-RNase III endonuclease domain were pooled, and ethylenediaminetetraacetic acid (EDTA) was added to a final concentration of 1 mM. The pooled fractions were concentrated by diafiltration and fractionated on a HiPrep 26/60 Sephacryl S-100 HR column (Amersham Pharmacia Biotech) equilibrated in buffer A containing 1 mM EDTA. Fractions containing RNase III endonuclease domain were pooled, dialyzed against 25 mM Tris (pH 7.5) 600 mM NaCl buffer, and concentrated

to 27 mg ml^{-1} (determined spectrophotometrically using a molar extinction coefficient of 14650 M^{-1} cm^{-1}). Aliquots were flash-frozen with liquid nitrogen and stored at 193K until use. The final product was judged to be >95% pure, on the basis of silver staining after sodium dodecyl sulfate-polyacrylamide gel electrophoresis (data not shown). The molecular weight of the Aa-RNase III endonuclease domain was confirmed by electrospray mass spectrometry.

Crystallization, Derivatization, and Complex Formation

Crystals of the ligand-free Aa-RNase III endonuclease domain were grown using the hanging-drop vapor diffusion method at 19 ± 1°C. The protein stock solution contained 13 mg/ml protein and 0.6 M NaCl in 25 mM Tris-HCl (pH 7.5); the reservoir solution consisted of 30% (w/v) PEG4000 and 0.2 M sodium acetate in 0.1 M Tris-HCl (pH 8.5). The drops contained equal volumes of protein and reservoir solutions. The microcrystals appeared overnight and reached the size suitable for X-ray analysis after 6–7 days (Table 1).

For the use of multiple isomorphous replacement (MIR) method, two heavy-atom derivatives were obtained by soaking the native crystals in heavy-atom-containing solutions for 24 hr at room temperature. The well solution of crystallization was used to make the soaking solution. Saturated heavy-atom solution was made first and then diluted to 50% saturation. Gold-sodium thiosulfate and uranyl acetate were used as heavy-atom donors for the Au and U derivatives, respectively.

Crystals of the complex of Aa-RNase III endonuclease domain with Mn^{2+} or Mg^{2+} ions were grown under the same condition as the ligand-free crystals, except that the reservoir solution contained 2 mM $MnCl_2$ or $MgCl_2$ in addition. The complex crystals appeared overnight from the precipitated material. After 1 week, the size of the crystals was suitable for X-ray data acquisition (Table 1).

X-Ray Data Collection and Processing

The X-ray diffraction data were collected at the National Synchrotron Light Source (Brookhaven National Laboratory, Upton, NY) at cryogenic temperature maintained with an Oxford Cryogenic System. The native, U derivative, and Mn^{2+} complex data sets were collected with an ADSC Quantum-4 CCD detector mounted at beamline X9B; the Au derivative data set was collected using a Brandeis four-module CCD-based detector at beamline X12C. Data processing was carried out with HKL2000 [46]. Crystal data and statistics of data processing are summarized in Table 1.

Structure Solution and Refinement

The ligand-free structure was solved by MIR phasing. Heavy-atom sites (Table 1) were derived from difference Patterson syntheses using SOLVE [47]. Heavy-atom site refinement, MIR phase calculation, and density modification with the solvent flipping procedure were carried out with SHARP [48]. Further density modification with noncrystallographic symmetry (NCS) averaging was performed using the CCP4 package [49]. The resulting MIR map was of high quality, allowing 88% of the structure to be built. Tracing and model building were done with O [50]. Initial refinement was carried out using CNS [51] with 5% reflections for R_{free} calculations. Bulk solvent correction was used, and loose NCS restraints between the two crystallographically independent molecules were applied. The difference electron density calculated after each round of refinement revealed the position of several missing residues. A few cycles of model building and refinement resulted in a model containing residues 1–147. No density was observed for the N-terminal glycine and the C-terminal His-tag residues. The final stage of refinement and the addition of solvent molecules were performed using SHELXL-97 [52] without any NCS restraints. The statistics of MIR phasing and refinement are summarized in Table 2.

The structure of the Mn^{2+} complex of Aa-RNase III endonuclease domain was solved using molecular replacement (MR). The dimer of ligand-free structure (PDB entry 1i4s, this work) without solvent atoms was the search model for AMoRe [53], resulting in a solution consisting of two dimeric complexes (Table 2). The structure was initially refined with CNS [51] with NCS restraints for the two independent dimers in the asymmetric unit. The NCS restraints were not used during the final stage of refinement using SHELXL-97 [52]. Bulk solvent correction was employed in all refinement cycles. Model building was done with O [50]. The difference electron density clearly revealed the N-terminal nonnative glycine residue for each polypeptide chain. Four Mn^{2+} ions were found in the asymmetric unit, with one Mn^{2+} per polypeptide chain. The His-tags were partially visible from the electron density only for molecule B in one dimer and for molecule A in the other. The average B factor for the structure including solvent molecules is 32.9 $Å^2$, which is consistent with the estimated value using the Wilson plot (28.3 $Å^2$). The refinement statistics and structure analysis are summarized in Table 2.

Functional Analysis of the *rnc* Mutants

The *E. coli rnc* gene in pACS21 [54] was mutagenized using the QuikChange site-directed mutagenesis kit (Stratagene) according to the manufacturer's protocol. The following amino acid substitutions were made: E38V, E38Q, F40G, F40D, F40M, F40R, F40W, D45A, E65A, and E65P (see Figure 1 for the corresponding amino acid residue numbers in Aa-RNase III).

The functional activity of *rnc* mutants was analyzed in the λ*N-lacZ* gene expression assay [33, 34]. The assay is based on the ability of RNase III to cleave an in vitro-engineered reporter gene construct introduced into *E. coli* cells. It includes a natural RNase III substrate derived from λ that tightly regulates the expression of the *lacZ* reporter gene. The *lacZ* gene can be expressed efficiently only when this λ element is cleaved by RNase III; the level of *lacZ* expression also depends on the activity of RNase III. Therefore, this assay allows one to quantitatively measure the cleavage activity of RNase III in its natural environment and produce data that adequately reflect the ability of RNase III to cleave RNA. The pACS21 and pSDF701 [34] plasmids carrying the wild-type *rnc* and *rnc70*, respectively, were used as controls throughout these experiments.

Molecular Modeling Studies

Molecular modeling studies were carried out with X-PLOR 3.851 [55] and O 6.0 [56] on an Octane1 workstation. The model of full-length Aa-RNase III in complex with Mg^{2+} and dsRNA was built based on the crystal structures of the *A. aeolicus* endonuclease domain/Mn^{2+} complex (this work) and the *X. laevis* dsRBD/dsRNA complex [29]. Solvent molecules were excluded from both structures. The structure of the *X. laevis* dsRBD/dsRNA complex ([29], Figure 6a) was used to create the coordinates of an *A. aeolicus* dsRBD with a dsRNA substrate containing 23 bp (Figure 6b). Based on the fact that RNase III is Mg^{2+} dependent [2–4, 16] and that Mg^{2+} binds to functionally essential residues in the compound active center (Figure 4a, this work), we assumed that the metal ions mediate dsRNA binding by neutralizing the negative charges of the active site residues. Accordingly, the *A. aeolicus* dsRDB/dsRNA model was oriented with respect to the *A. aeolicus* endonuclease domain/Mn^{2+} complex such that dsRNA was parallel with the dsRNA-accommodating valley and the N terminus of dsRBD was in the vicinity of the C terminus of the endonuclease domain. The resulting model contained two endonuclease domains, one dsRBD, a 23-bp dsRNA, and two Mn^{2+} ions that were given the identity of Mg^{2+} (Figure 6c and 6d). The dsRBD was then transformed to add the second dsRBD of the dimer using the transformation matrix between the two endonuclease domains. In the resulting dimer of Aa-RNase III/Mg^{2+}/dsRNA, the dsRBD-dsRNA interactions as found in the crystal structure [29] were maintained for both dsRBDs (Figure 6e and 6f). To complete the entire length of Aa-RNase III, the three missing residues (148–150, see Figures 1b and 6f) were modeled between endonuclease domain and dsRBD; two residues (191–192, see Figures 1b and 6b) were inserted into dsRBD. The 148–150 insertions between the two domains reasonably connect the C-terminal helix (α7) of endonuclease domain and the N-terminal helix (α1) of dsRBD; the 191–192 insertions simply extend the β hairpin end of β2–β3 (Figure 6b and 6f). The complete model, containing two full-length Aa-RNase III molecules, two Mg^{2+} ions, and a 23-bp dsRNA, was subject to mild energy minimization to eliminate extreme clashes. The Engh and Huber [57] geometric parameters were used as the basis of the force field.

Acknowledgments

We thank Drs. Z. Dauter, K.R. Rajashankar, R.M. Sweet, A.M. Saxena, and A. Evdokimov for their help and suggestions during data

collection and processing at the synchrotron beamlines X9B and X12C, National Synchrotron Light Source, Brookhaven National Laboratory, and Dr. A. Evdokimov for his help in MIR phasing. We thank Drs. D. Yu, E. Anderson, and L. Reshetnikova for their contribution in the early stages of protein expression, purification, and crystallization trials and A. Wlodawer and A. Oppenheim for insightful discussions and critical reading of the manuscript.

Received: November 2, 2001
Accepted: November 7, 2001

References

1. Robertson, H.D., Webster, R.E., and Zinder, N.D. (1968). Purification and properties of ribonuclease III from *Escherichia coli*. J. Biol. Chem. *243*, 82–91.
2. Court, D. (1993). RNA processing and degradation by RNase III. In Control of Messenger RNA Stability, J.G. Belasco and G. Braverman, eds. (New York: Academic Press), pp. 71–116.
3. Nicholson, A.W. (1996). Structure, reactivity, and biology of double-stranded RNA. Prog. Nucleic Acid Res. Mol. Biol. *52*, 1–65.
4. Nicholson, A.W. (1999). Function, mechanism and regulation of bacterial ribonucleases. FEMS Microbiol. Rev. *23*, 371–390.
5. Krainer, A. (1997). Eukaryotic mRNA Processing. (New York: IRL Press).
6. Filippov, V., Solovyev, V., Filippova, M., and Gill, S.S. (2000). A novel type of RNase III family proteins in eukaryotes. Gene *245*, 213–221.
7. Bernstein, E., Caudy, A.A., Hammond, S.M., and Hannon, G.J. (2001). Role for a bidentate ribonuclease in the initiation step of RNA interference. Nature *409*, 363–366.
8. Chen, S.M., Takiff, H.E., Barber, A.M., Dubois, G.C., Bardwell, J.C., and Court, D.L. (1990). Expression and characterization of RNase III and Era proteins. Products of the *rnc* operon of *Escherichia coli*. J. Biol. Chem. *265*, 2888–2895.
9. Robertson, H.D. (1990). *Escherichia coli* ribonuclease III. Methods Enzymol. *181*, 189–202.
10. Gitelman, D.R., and Apirion, D. (1980). The synthesis of some proteins is affected in RNA processing mutants of *Escherichia coli*. Biochem. Biophys. Res. Commun. *96*, 1063–1070.
11. Gegenheimer, P., and Apirion, D. (1980). Precursors to 16S and 23S ribosomal RNA from a ribonuclear III-strain of *Escherichia coli* contain intact RNase III processing sites. Nucleic Acids Res. *8*, 1873–1891.
12. Gegenheimer, P., and Apirion, D. (1981). Processing of procaryotic ribonucleic acid. Microbiol Rev. *45*, 502–541.
13. Dunn, J.J. (1976). RNase III cleavage of single-stranded RNA. Effect of ionic strength on the fidelity of cleavage. J. Biol. Chem. *251*, 3807–3814.
14. Krinke, L., and Wulff, D.L. (1987). OOP RNA, produced from multicopy plasmids, inhibits lambda *cII* gene expression through an RNase III-dependent mechanism. Genes Dev. *1*, 1005–1013.
15. Krinke, L., and Wulff, D.L. (1990). The cleavage specificity of RNase III. Nucleic Acids Res. *18*, 4809–4815.
16. Dunn, J.J. (1982). Ribonuclease III. In The Enzymes, P. Boyer, ed. (New York: Academic Press), pp. 485–499.
17. Robertson, H.D. (1982). *Escherichia coli* ribonuclease III cleavage sites. Cell *30*, 669–672.
18. Langenberg, W.G., Zhang, L., Court, D.L., Giunchedi, L., and Mitra, A. (1997). Transgenic tobacco plants expressing the bacterial rnc gene resist virus infection. Mol. Breeding *3*, 391–399.
19. Hamilton, A.J., and Baulcombe, D.C. (1999). A species of small antisense RNA in posttranscriptional gene silencing in plants. Science *286*, 950–952.
20. Hammond, S.M., Bernstein, E., Beach, D., and Hannon, G.J. (2000). An RNA-directed nuclease mediates post-transcriptional gene silencing in *Drosophila* cells. Nature *404*, 293–296.
21. Grishok, A., et al., and Mello, C.C. (2001). Genes and mechanisms related to RNA interference regulate expression of the small temporal RNAs that control *C. elegans* developmental timing. Cell *106*, 23–34.
22. Hutvagner, G., McLachlan, J., Pasquinelli, A.E., Balint, E., Tuschl, T., and Zamore, P.D. (2001). A cellular function for the RNA-interference enzyme Dicer in the maturation of the let-7 small temporal RNA. Science *293*, 834–838.
23. Wu, H., Xu, H., Miraglia, L.J., and Crooke, S.T. (2000). Human RNase III is a 160-kDa protein involved in preribosomal RNA processing. J. Biol. Chem. *275*, 36957–36965.
24. Carthew, R.W. (2001). Gene silencing by double-stranded RNA. Curr. Opin. Cell Biol. *13*, 244–248.
25. Kharrat, A., Macias, M.J., Gibson, T.J., Nilges, M., and Pastore, A. (1995). Structure of the dsRNA binding domain of *E. coli* RNase III. EMBO J. *14*, 3572–3584.
26. Bycroft, M., Grunert, S., Murzin, A.G., Proctor, M., and St Johnston, D. (1995). NMR solution structure of a dsRNA binding domain from *Drosophila staufen* protein reveals homology to the N-terminal domain of ribosomal protein S5. EMBO J. *14*, 3563–3571.
27. Nanduri, S., Carpick, B.W., Yang, Y., Williams, B.R., and Qin, J. (1998). Structure of the double-stranded RNA-binding domain of the protein kinase PKR reveals the molecular basis of its dsRNA-mediated activation. EMBO J. *17*, 5458–5465.
28. Ramos, A., et al., and Varani, G. (2000). RNA recognition by a Staufen double-stranded RNA-binding domain. EMBO J. *19*, 997–1009.
29. Ryter, J.M., and Schultz, S.C. (1998). Molecular basis of double-stranded RNA-protein interactions: structure of a dsRNA-binding domain complexed with dsRNA. EMBO J. *17*, 7505–7513.
30. Ji, X., Zhang, P., Armstrong, R.N., and Gilliland, G.L. (1992). The three-dimensional structure of a glutathione S-transferase from the mu gene class. Structural analysis of the binary complex of isoenzyme 3–3 and glutathione at 2.2 Å resolution. Biochemistry *31*, 10169–10184.
31. Armstrong, R.N. (1997). Structure, catalytic mechanism, and evolution of the glutathione transferases. Chem. Res. Toxicol. *10*, 2–18.
32. Ji, X., et al., and Zimniak, P. (1997). Structure and function of the xenobiotic substrate-binding site and location of a potential non-substrate-binding site in a class pi glutathione S-transferase. Biochemistry *36*, 9690–9702.
33. Kameyama, L., Fernandez, L., Court, D.L., and Guarneros, G. (1991). RNase III activation of bacteriophage lambda N synthesis. Mol. Microbiol. *5*, 2953–2963.
34. Dasgupta, S., et al., and Court, D.L. (1998). Genetic uncoupling of the dsRNA-binding and RNA cleavage activities of the *Escherichia coli* endoribonuclease RNase III - the effect of dsRNA binding on gene expression. Mol. Microbiol. *28*, 629–640.
35. Li, H., and Nicholson, A.W. (1996). Defining the enzyme binding domain of a ribonuclease III processing signal. Ethylation interference and hydroxyl radical footprinting using catalytically inactive RNase III mutants. EMBO J. *15*, 1421–1433.
36. Sun, W., and Nicholson, A.W. (2001). Mechanism of action of *Escherichia coli* ribonuclease III. Stringent chemical requirement for the glutamic acid 117 side chain and Mn(2+) rescue of the Glu117Asp mutant. Biochemistry *40*, 5102–5110.
37. Inada, T., Kawakami, K., Chen, S.M., Takiff, H.E., Court, D.L., and Nakamura, Y. (1989). Temperature-sensitive lethal mutant of ERA, a G protein in *Escherichia coli*. J. Bacteriol. *171*, 5017–5024.
38. Davidov, Y., Rahat, A., Flechner, I., and Pines, O. (1993). Characterization of the *rnc-97* mutation of RNase III: a glycine to glutamate substitution increases the requirement for magnesium ions. J. Gen. Microbiol. *139*, 717–724.
39. Crouch, R.J. (1974). Ribonuclease 3 does not degrade deoxyribonucleic acid-ribonucleic acid hybrids. J. Biol. Chem. *249*, 1314–1316.
40. Robertson, H.D., and Dunn, J.J. (1975). Ribonucleic acid processing activity of *Escherichia coli* ribonuclease III. J. Biol. Chem. *250*, 3050–3056.
41. Montgomery, M.K., Xu, S., and Fire, A. (1998). RNA as a target of double-stranded RNA-mediated genetic interference in *Caenorhabditis elegans*. Proc. Natl. Acad. Sci. USA *95*, 15502–15507.
42. Montgomery, M.K., and Fire, A. (1998). Double-stranded RNA as a mediator in sequence-specific genetic silencing and cosuppression. Trends Genet. *14*, 255–258.

43. Fire, A., Xu, S., Montgomery, M.K., Kostas, S.A., Driver, S.E., and Mello, C.C. (1998). Potent and specific genetic interference by double-stranded RNA in *Caenorhabditis elegans*. Nature *391*, 806–811.
44. Evdokimov, A.G., Anderson, D.E., Routzahn, K.M., and Waugh, D.S. (2000). Overproduction, purification, crystallization and preliminary X-ray diffraction analysis of YopM, an essential virulence factor extruded by the plague bacterium *Yersinia pestis*. Acta Crystallogr. D *56*, 1676–1679.
45. Miller, J.H. (1972). Experiments in Molecular Genetics. (Cold Spring Harbor, NY: Cold Spring Harbor Laboratory).
46. Otwinowski, Z., and Minor, W. (1997). Processing of X-ray diffraction data collected in oscillation mode. Methods Enzymol. *276*, 307–326.
47. Terwilliger, T.C., and Berendzen, J. (1999). Automated MAD and MIR structure solution. Acta Crystallogr. D *55*, 849–861.
48. de La Fortelle, E., and Bricogne, G. (1997). Maximum-likelihood heavy-atom parameter refinement for multiple isomorphous replacement and multiwavelength anomalous diffraction methods. Methods Enzymol. *276*, 472–494.
49. Collaborative Computational Project Number 4 (1994). The CCP4 suite: programs for protein crystallography. Acta Crystallogr. D *50*, 760–763.
50. Jones, T.A., Zou, J.Y., Cowan, S.W., and Kjeldgaard, M. (1991). Improved methods for building protein models in electron density maps and the location of errors in these models. Acta Crystallogr. A *47*, 110–119.
51. Brünger, A.T., et al., and Warren, G.L. (1998). Crystallography & NMR system: a new software suite for macromolecular structure determination. Acta Crystallogr. D *54*, 905–921.
52. Sheldrick, G.M., and Schneider, T.R. (1997). SHELXL: high-resolution refinement. Methods Enzymol. *277*, 319–343.
53. Navaza, J. (1994). An automated package for molecular replacement. Acta Crystallogr. A *50*, 157–163.
54. Takiff, H.E., Chen, S.M., and Court, D.L. (1989). Genetic analysis of the *rnc* operon of *Escherichia coli*. J Bacteriol. *171*, 2581–2590.
55. Brünger, A.T., and Rice, L.M. (1997). Crystallographic refinement by simulated annealing: methods and applications. Methods Enzymol. *277*, 243–269.
56. Jones, T.A., and Kjeldgaard, M. (1997). Electron-density map interpretation. Methods Enzymol. *277*, 173–208.
57. Engh, R.A., and Huber, R. (1991). Accurate bond and angle parameters for X-ray protein structure refinement. Acta Crystallogr. A *47*, 392–400.
58. Nashimoto, H., and Uchida, H. (1985). DNA sequencing of the *Escherichia coli* ribonuclease III gene and its mutations. Mol. Gen. Genet. *201*, 25–29.
59. Bardwell, J.C., Regnier, P., Chen, S.M., Nakamura, Y., Grunberg-Manago, M., and Court, D.L. (1989). Autoregulation of RNase III operon by mRNA processing. EMBO J. *8*, 3401–3407.
60. Inada, T., and Nakamura, Y. (1995). Lethal double-stranded RNA processing activity of ribonuclease III in the absence of suhB protein of *Escherichia coli*. Biochimie *77*, 294–302.
61. Kraulis, P.J. (1991). MOLSCRIPT: a program to produce both detailed and schematic plots of protein structures. J. Appl. Crystallogr. *24*, 946–950.
62. Nicholls, A., Sharp, K.A., and Honig, B. (1991). Protein folding and association: insights from the interfacial and thermodynamic properties of hydrocarbons. Proteins Struct. Funct. Genet. *11*, 281–296.
63. Merritt, E.A., and Bacon, D.J. (1997). Raster3D: photorealistic molecular graphics. Methods Enzymol. *277*, 505–524.

Accession Numbers

The coordinates and structure factors have been deposited in the Protein Data Bank. (The Rutgers State University of New Jersey, NJ, USA) with the accession codes 1i4s (ligand-free) and 1jfz (Mn^{2+} complex).